Optical Excitations and Field Enhancement in Short Graphene Nanoribbons

Caterina Cocchi,*[†,‡] Deborah Prezzi,*[†] Alice Ruini,[†,‡] Enrico Benassi,[†] Marilia J. Caldas,[¶] Stefano Corni,[†] and Elisa Molinari[†,‡]

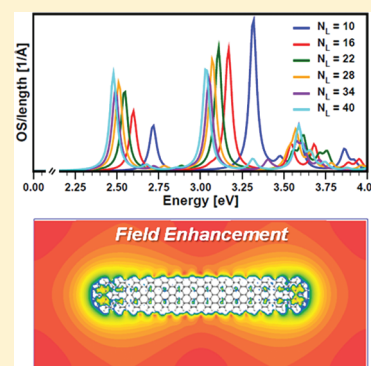[†]Centro S3, CNR-Istituto Nanoscienze, I-41125 Modena, Italy
[‡]Dipartimento di Fisica, Università di Modena e Reggio Emilia, I-41125 Modena, Italy
[¶]Instituto de Física, Universidade de São Paulo, 05508-900 São Paulo, SP, Brazil

S *Supporting Information*

ABSTRACT: The optical excitations of elongated graphene nanoflakes of finite length are investigated theoretically through quantum chemistry semiempirical approaches. The spectra and the resulting dipole fields are analyzed, accounting in full atomistic details for quantum confinement effects, which are crucial in the nanoscale regime. We find that the optical spectra of these nanostructures are dominated at low energy by excitations with strong intensity, comprised of characteristic coherent combinations of a few single-particle transitions with comparable weight. They give rise to stationary collective oscillations of the photoexcited carrier density extending throughout the flake and to a strong dipole and field enhancement. This behavior is robust with respect to width and length variations, thus ensuring tunability in a large frequency range. The implications for nanoantennas and other nanoplasmonic applications are discussed for realistic geometries.

SECTION: Nanoparticles and Nanostructures

In the last few years, remarkable interest has grown for nanoplasmonics and the perspectives it offers to merge electronics and photonics at the nanoscale.[1,2] A wide range of potential applications can be designed, including sensing and spectroscopic techniques,[3–6] fabrication of nanoantennas[7–11] and light emitters,[12,13] as well as beyond-THz optical devices or solar energy conversion systems.[14–16] While great attention has been devoted to metal nanoparticles due to the relative ease to produce them and to their possibility to support surface modes,[17–19] new materials and metamaterials are now being explored,[20,21] which, in addition to enhanced optical responses, are able to optimize circuit integration and reduce losses. Graphene has proved to have unique electronic and mechanical properties[22] and has been more recently investigated also for photonics and optoelectronics.[23–25] In the field of (nano)-plasmonics, so far, most emphasis has been devoted to the spectroscopy of plasmons in extended graphene, either doped or undoped,[26–32] and to the large lifetimes of their excitations compared to those of conventional metals.[30,33] Some interesting predictions, mostly based on macroscopic models, have been proposed for plasmonics in spatially modulated graphene of the micrometer and submicrometer size range.[32,34–38]

Here, we focus on graphene in a completely different regime, typical of nanoscale structures, where an optical gap opens as a consequence of quantum confinement, and we show that field enhancement effects can also be seen. This regime has become particularly exciting in view of the recent production of controlled graphene wires by chemical routes.[39–42] We consider the case of self-standing elongated graphene nano-flakes (GNFs) with H-terminated edges, which we analyze by applying a fully microscopic quantum chemical approach. These flakes can be thought of as finite portions of armchair-edged graphene nanoribbons (GNRs)[43] (see Figure 1a) of variable widths and lengths. We focus on the optical properties, which are sensitive to the structural details of the system, namely length and width modulation, by computing their UV−vis spectra. In the low-energy region, intense and tunable peaks are recognized, characterized by a coherent coupling of transitions that yield "collective" excitations with a strong transition dipole. The local field enhancement produced by these large dipole excitations is discussed for a prototypical flake of subnanometer width and nanometer length.

To investigate the nature of these optical excitations, their microscopic origin and their size-dependent trends, we adopt the semiempirical Hartree−Fock-based method ZINDO, which implements the configuration-interaction (CI) procedure including single excitations only (S).[44] This method is known to provide reliable results for the optical spectra of aromatic molecules.[45–48] All calculations are performed starting from optimized geometries obtained with AM1,[49,50] used also for the calculation of mean-field ground-state properties.
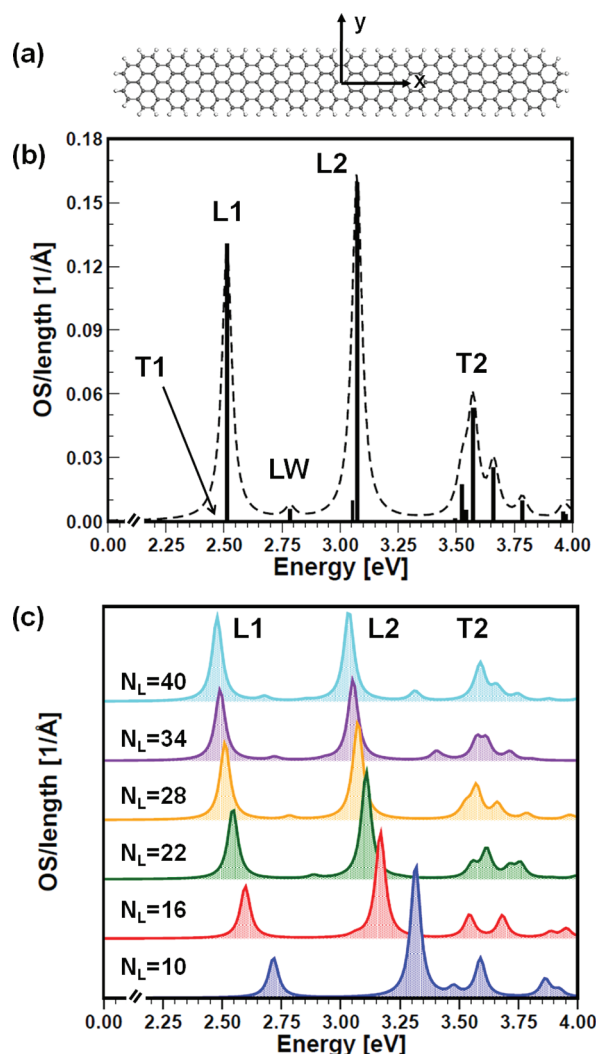
Figure 1. (a) Ball-and-stick model of a prototypical elongated graphene flake, characterized by length parameter $N_L = 28$ (x direction) and width parameter $N_W = 7$ (y direction). Edge atoms are passivated with H (white balls). (b) Optical spectrum (dashed line) calculated for the system in (a); the oscillator strength (OS) of individual excitations is indicated by black bars. The main excitations are labeled according to their polarization with respect to the long axis of the system (x), that is, L for longitudinal and T for transverse polarization. (c) Optical spectra of a series of graphene flakes of fixed width ($N_W = 7$) and variable length, from 24 to 88 Å, labeled after their length parameter N_L, ranging from 10 to 40. The OS is normalized with respect to the flake length in both (b) and (c). All spectra are obtained by introducing a Lorentzian broadening of 25 meV.

The analysis of the optical properties is carried out for a series of prototypical short GNRs (or GNFs) of fixed width (~7.3 Å) and variable length (from 24 to 88 Å). Following the standard notation for armchair GNRs,[43] these structures can be characterized by a width parameter N_W, which indicates the number of dimeric lines along the zigzag direction (y axis). In addition, we here introduce a length parameter N_L that corresponds to the number of zigzag chains in the armchair direction (x axis), excluding the ends. As shown in the model structure of Figure 1a, the flake edges are passivated with H atoms, and the flake ends are shaped to minimize the zigzag edge contributions.[51,52] The structure of a prototypical flake with $N_W = 7$ and $N_L = 28$ is displayed in Figure 1a, and its UV–

vis spectrum (dashed line) is shown in Figure 1b, where the oscillator strength (OSs) of the individual optical excitations are indicated by black bars. The optical spectrum is dominated by three intense peaks: the first two, L1 and L2, correspond to excitations with a large transition dipole along the x axis of the system (L stands for longitudinally polarized), and the third peak is found at higher energy and is dominated by the excitation T2, which shows a transverse polarization (y direction) with respect to the long axis of the system. In addition to these, we also find a transversely polarized excitation T1 with negligible oscillator strength below the first peak L1 and a weak longitudinally polarized excitation (LW) between L1 and L2. Figure 1c displays the calculated UV–vis spectra for GNFs of the same width ($N_W = 7$) and increasing length, with N_L ranging from 10 to 40. The main features described for the case of $N_L = 28$ are maintained along the flake series, except for L1 becoming the lowest-energy excitation in place of T1 for the longest GNF ($N_L = 40$); this is a signature of the approaching behavior of quasi-1D armchair graphene nanoribbons (AGNRs).[53] Moreover, as a result of confinement, we find an overall red shift of L1 and L2, with the optical gap decreasing from 3.14 to 2.48 eV. The energy difference between these longitudinal excitations is almost unaffected upon flake length increase, ranging from about 0.55 ($N_L = 40$) to 0.60 eV ($N_L = 10$). As expected, the energy of T1 and T2 does not vary considerably with length because they are polarized along the flake width, kept fixed. At increasing length, we also notice a significant transfer of OS to the lowest-energy peak L1, which tends to saturate for the longest flake, again similarly to the behavior of infinite nanoribbons.[53]

To gain further insight into the nature of these spectral features, we analyze the composition of all low-energy excitations in terms of molecular orbital (MO) transitions and CI weights. The numerical details are presented in the Supporting Information (Table S1) for a few selected cases; here, we focus again on $N_L = 28$, starting from the first bright excitation L1. As illustrated in Figure 2, this excitation arises from the coherent combination of single-particle transitions involving several harmonics of the same states. Note that while in shorter flakes, the HOMO → LUMO transition contributes for most of the weight, in longer structures, several higher harmonics enter the composition with comparable weights. The fact that transitions between occupied and virtual MOs with the same envelope function modulation concur to form the excitation helps explaining the large OS observed, as this mechanism tends to maximize the wave function overlap. The spatial extension of the MOs increases with their energy distance from the frontier orbitals, further contributing to the large transition dipole. This effect is made particularly evident by plotting the transition density of the excitation, defined as

$$\rho^{0p}(\mathbf{r}) = \sum_{ia} C_{ia}^{p} \phi_i(\mathbf{r}) \phi_a^*(\mathbf{r})$$

(1)

where C_{ia}^{p} are the CI coefficients of the pth excited state, corresponding to single excitations from the occupied ϕ_i to virtual ϕ_a orbitals.[54] From Figure 2a, we notice that the density extends homogeneously over the entire structure with an underlying dipolar character and is not concentrated just to the central portion. This is evident also by inspecting the contour plot of the corresponding electric potential, pictorially represented in Figure 3.
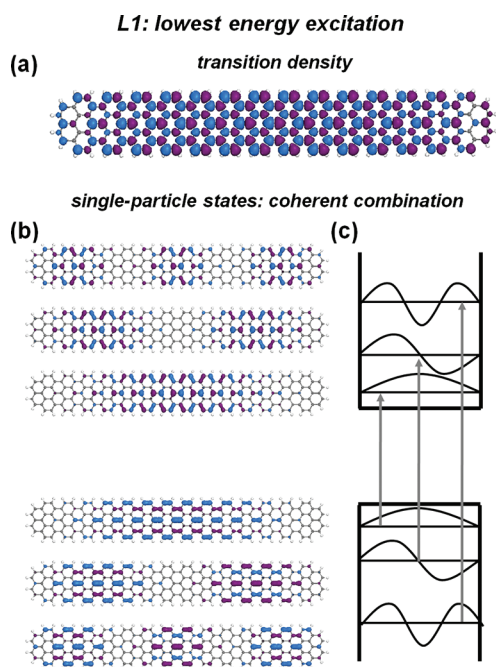
L1: lowest energy excitation

(a)

transition density

single-particle states: coherent combination

(b) **(c)**

Figure 2. Lowest-energy excitation L1 of the N_L = 28 graphene flake shown in Figure 1a. (a) Transition density computed according to eq 1. (b) Single-particle wave functions mostly contributing to L1. The lowest-energy excitation L1 is obtained from a coherent superposition of single-particle transitions, as indicated in (c).
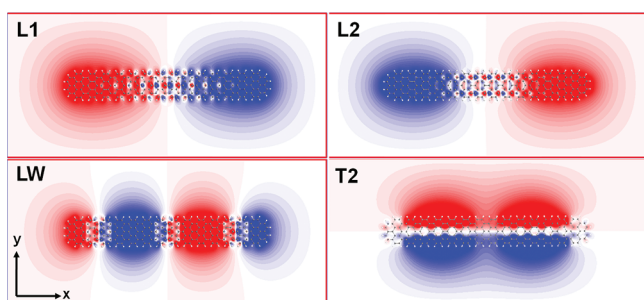
L1 L2

LW T2

Figure 3. Pictorial view of the electric potential generated by the transition density relative to the excitations L1, L2, LW, and T2 of the N_L = 28 flake.

As expected from their polarization, L1 and L2 have a large dipole oriented along x, while that of T2 is along y. As shown for L1 in Figure 2, also L2 and T2 arise from combinations of transitions between states with the same envelope function modulation. On the contrary, LW is mainly composed of transitions involving MOs with a different number of nodes. This gives rise to a multipolar modulation in the electric potential, as shown in Figure 3, and leads to the weaker intensity observed for this excitation.

The large dipole strength and the "beyond-single-particle" nature of L1 and L2 recall the main features related to collective plasmonic excitations in small metal clusters, as analyzed by means of atomistic methods.[55−58] We thus calculate for our systems a quantity that is usually adopted for the characterization of plasmonic excitations, that is, the local enhancement of an electromagnetic field incident on the system. To this end, we approximate the flake response function, at resonance conditions, via the electronic density variation $\delta\rho(\omega_{0p};\mathbf{r})$

induced by the periodic external electric field $\mathbf{E}_0 \exp(-i\omega_{0p}t)$, given by

$$\delta\rho(\omega_{0p};\ \mathbf{r}) = -\frac{\rho^{0p}(\mathbf{r})}{i\hbar\Gamma_p}\mu^{0p}\cdot\mathbf{E}_0$$

(2)

Here $\boldsymbol{\mu}^{0p}$ is the transition dipole for the excitation to the in-resonance p state, and Γ_p is the corresponding decay rate, related to the intrinsic absorption bandwidth. Details on the derivation of eq 2 are given in the Supporting Information. The oscillating charge distribution $\delta\rho(\omega_{0p};\mathbf{r})$ brings about an additional electric field $\mathbf{E}_e(\mathbf{r}) \exp(-i\omega_{0p}t)$, leading to an overall enhanced electric field $(\mathbf{E}_0 + \mathbf{E}_e)$ nearby the graphene flake. The transition dipole $\boldsymbol{\mu}^{0p}$ is a straight result from the calculation, while Γ_p is a critical parameter in determining the maximum enhancement (the larger this value, the smaller the enhancement, as shown in eq 2). The field enhancement is obtained by deriving the electric Coulomb potential generated by the transition density and is expressed in units of E_0 (E_e/E_0). Since experimental data are not yet available for graphene nanoflakes such as those examined here, we adopt in the figures a conservative value Γ_p = 25 meV, chosen from the spectral line widths measured for single-wall carbon nanotubes (SWCNTs) at room temperature in solution.[59] Due to the critical dependence of the field enhancement on the choice of Γ_p (see eq 2), it is worth noting that the field enhancement shown in Figure 4 would increase of over one order of magnitude for
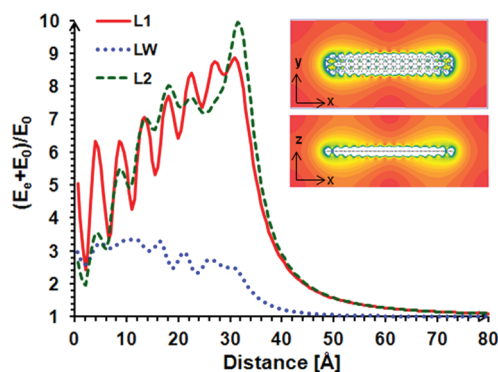
Figure 4. Field enhancement of longitudinally polarized excitations L1, L2, and LW of the N_W = 7 and N_L = 28 graphene nanoflake computed along the flake axis, at 3.3 Å from its plane. Close to the flake center, above its surface, the field enhancement is susceptible of the transition density modulation (see Figure 2a). In the inset, a pictorial sketch of the field enhancement contour plot in (x,y) and (x,z) views. Notice that the values of the field enhancement are sensitive to the choice of Γ_p, according to eq 2; here, a conservative value of Γ_p = 25 meV is adopted.

$\Gamma_p \approx 1$ meV, as found for suspended SWCNTs at low temperature.[60] In Figure 4, we show the field enhancement produced by the three main longitudinal excitations (L1, LW, and L2) identified in Figure 1b for the GNF of N_W = 7 and N_L = 28, computed along the flake longitudinal (x) axis, at a distance of 3.3 Å from the basal plane (see Figure 5b). The oscillating character of the curves in the region above the flake surface is due to the transition density modulation (see Figure 2a). Beyond the flake border, the oscillations disappear, and at distance much larger than the flake half-length (∼30 Å), the field enhancement assumes a Coulomb-like decay, proportional to $1/r^2$. According to the OS of the corresponding excitations,
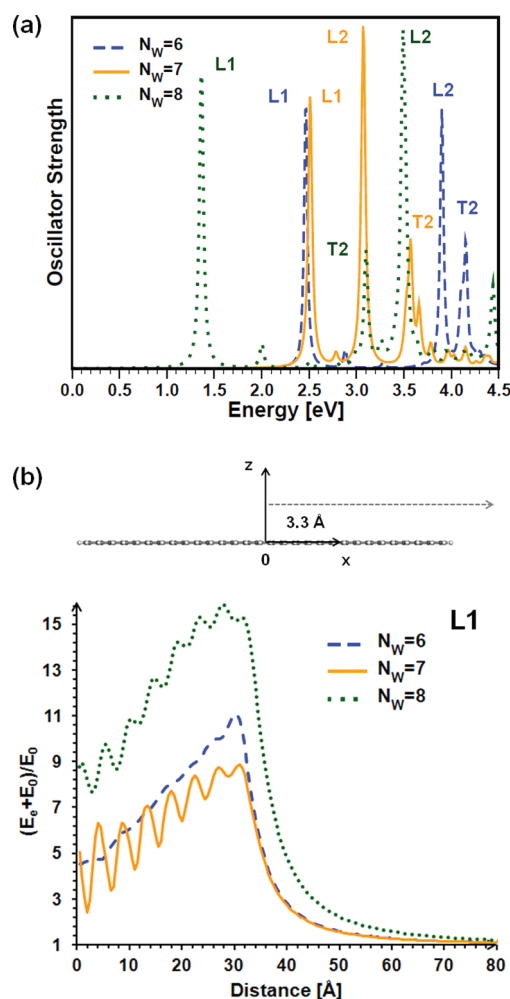
Figure 5. (a) UV−vis spectra of a series of graphene flake of fixed length ($N_L = 28$) and variable width, with N_W ranging from 6 to 8. A Lorentzian broadening of 25 meV is introduced. (b) Field enhancement of L1 excitations along the flake longitudinal axis, at a distance of 3.3 Å from its basal plane, according to the scheme reported on top of the graph. Notice that the values of the field enhancement are sensitive to the choice of Γ_p, according to eq 2; here, a conservative value of $\Gamma_p = 25$ meV is adopted.

the field enhancements for L1 and L2 have comparable values, while that of LW is about three times lower.

Finally, we discuss the stability and the tunability of these optical properties with respect to length and width modulation. Focusing specifically on the lowest-energy peak L1, the computed values of field enhancement are basically independent of the ribbon length (see Supporting Information, Figure S1). On the other hand, it is well-known that both the electronic and optical properties of quasi-1D AGNRs are sensitive to width modulation.[53,61−64] Also for the finite flakes considered here, three families are identified,[50] characterized by different electronic gaps, with the smallest values pertaining to the $N_W = 3p + 2$ family (p integer). Here, we investigate two additional graphene flakes of width parameters of $N_W = 6$ and 8, keeping their length fixed at $N_L = 28$. As shown in Figure 5a, the three main peaks (L1, L2, and T2) observed for $N_W = 7$ are preserved in all families. While T2 red shifts at increasing width, as expected, the energy and the intensity of the longitudinal excitations L1 and L2 are closely related to the electronic properties of each family. In particular, the trend for the

electronic gaps[50] is reflected in the excitation energies of L1. The field enhancement computed for the L1 excitation of each GNF of different width is shown in Figure 5b; we find a distinctive enhancement for $N_W = 8$ compared to the other two, which already comes from the transition dipole moments of the individual single-particle excitations.

In summary, we have analyzed the optical excitations of finite graphene nanoribbons of subnanometer width and nanometer length. At low energy, the UV−vis spectra are dominated by intense excitations with longitudinal polarization with respect to the flake long axis. These are characterized by a "collective" character, coming from coherent superposition of MO transitions with the same envelope function modulation. The investigated excitations are tunable both in energy and intensity upon appropriate length and width ribbon modulation. The field enhancement computed for these excitations suggests the applicability of these systems as nanoantennas and in other optoelectronic and nanoplasmonic applications.

■ ASSOCIATED CONTENT

Ⓢ Supporting Information

We include the description of the main excitations, both longitudinally and transversally polarized, for selected graphene ribbons of variable length and width. The effects of length modulation on the field enhancement produced by the lowest-energy bright excitation are discussed, supported by a figure showing the corresponding curves for a few selected cases. Finally, the analytical expression of the field enhancement is analytically derived from the transition density on the basis of linear response theory. This material is available free of charge via the Internet at http://pubs.acs.org.

■ AUTHOR INFORMATION

Corresponding Author

*E-mail: caterina.cocchi@unimore.it (C.C.); deborah.prezzi@unimore.it (D.P.).

Notes

The authors declare no competing financial interest.

■ ACKNOWLEDGMENTS

■ REFERENCES

(1) Ozbay, E. Plasmonics: Merging Photonics and Electronics at Nanoscale Dimensions. *Science* **2006**, *311*, 189−193.

(2) Brongersma, M. L.; Shalaev, V. M. The Case for Plasmonics. *Science* **2010**, *328*, 440−441.

(3) Willets, K.; Van Duyne, R. Localized Surface Plasmon Resonance Spectroscopy and Sensing. *Annu. Rev. Phys. Chem.* **2007**, *58*, 267−297.

(4) Homola, J. Surface Plasmon Resonance Sensors for Detection of Chemical and Biological Species. *Chem. Rev.* **2008**, *108*, 462−493.

(5) Stewart, M. E.; Anderton, C. R.; Thompson, L. B.; Maria, J.; Gray, S. K.; Rogers, J. A.; Nuzzo, R. G. Nanostructured Plasmonic Sensors. *Chem. Rev.* **2008**, *108*, 494−521.

(6) Anker, J.; Hall, W.; Lyandres, O.; Shah, N.; Zhao, J.; Van Duyne, R. Biosensing with Plasmonic Nanosensors. *Nat. Mater.* **2008**, *7*, 442−453.

(7) Muehlschlegel, P.; Eisler, H.-J.; Martin, O. J. F.; Hecht, B.; Pohl, D. W. Resonant Optical Antennas. *Science* **2005**, *308*, 1607−1609.

(8) Schnell, M.; Garcia-Etxarri, A.; Huber, A.; Crozier, K.; Aizpurua, J.; Hillenbrand, R. Controlling the Near-Field Oscillations of Loaded Plasmonic Nanoantennas. *Nat. Photonics* **2009**, *3*, 287−291.

(9) Bharadwaj, P.; Deutsch, B.; Novotny, L. Optical Antennas. *Adv. Opt. Photonics* **2009**, *1*, 438−483.

(10) Gao, S.; Ueno, K.; Misawa, H. Plasmonic Antenna Effects on Photochemical Reactions. *Acc. Chem. Res.* **2011**, *44*, 251−260.

(11) Giannini, V.; Fernandez-Dominguez, A. I.; Heck, S. C.; Maier, S. A. Plasmonic Nanoantennas: Fundamentals and Their Use in Controlling the Radiative Properties of Nanoemitters. *Chem. Rev.* **2011**, *111*, 3888−3912.

(12) Bergman, D. J.; Stockman, M. I. Surface Plasmon Amplification by Stimulated Emission of Radiation: Quantum Generation of Coherent Surface Plasmons in Nanosystems. *Phys. Rev. Lett.* **2003**, *90*, 027402.

(13) Stockman, M. Spasers Explained. *Nat. Photonics* **2008**, *2*, 327−329.

(14) Polman, A. Plasmonics Applied. *Science* **2008**, *322*, 868−869.

(15) Dragoman, M.; Dragoman, D. Plasmonics: Applications to Nanoscale Terahertz and Optical Devices. *Prog. Quantum Electron.* **2008**, *32*, 1−41.

(16) Schuller, J.; Barnard, E.; Cai, W.; Jun, Y.; White, J.; Brongersma, M. Plasmonics for Extreme Light Concentration and Manipulation. *Nat. Mater.* **2010**, *9*, 193−204.

(17) Kelly, K.; Coronado, E.; Zhao, L.; Schatz, G. The Optical Properties of Metal Nanoparticles: the Influence of Size, Shape, and Dielectric Environment. *J. Phys. Chem. B* **2003**, *107*, 668−677.

(18) Barnes, W.; Dereux, A.; Ebbesen, T. Surface Plasmon Subwavelength Optics. *Nature* **2003**, *424*, 824−830.

(19) Lal, S.; Link, S.; Halas, N. Nano-Optics from Sensing to Waveguiding. *Nat. Photonics* **2007**, *1*, 641−648.

(20) Konstantatos, G.; Sargent, E. Nanostructured Materials for Photon Detection. *Nat. Nanotechnol.* **2010**, *5*, 391−400.

(21) West, P.; Ishii, S.; Naik, G.; Emani, N.; Shalev, V.; Boltasseva, A. Searching for Better Plasmonic Materials. *Laser Photonics Rev.* **2010**, *4*, 795−808.

(22) Castro Neto, A. H.; Guinea, F.; Peres, N. M. R.; Novoselov, K. S.; Geim, A. K. The Electronic Properties of Graphene. *Rev. Mod. Phys.* **2009**, *81*, 109−162.

(23) Benisty, H. Graphene Nanoribbons: Photonic Crystal Waveguide Analogy and Minigap Stripes. *Phys. Rev. B* **2009**, *79*, 155409.

(24) Avouris, P. Graphene: Electronic and Photonic Properties and Devices. *Nano Lett.* **2010**, *10*, 4285−4294.

(25) Bonaccorso, F.; Sun, Z.; Hasan, T.; Ferrari, A. Graphene Photonics and Optoelectronics. *Nat. Photonics* **2010**, *4*, 611−622.

(26) Hwang, E.; Sarma, S. Dielectric Function, Screening, and Plasmons in Two-Dimensional Graphene. *Phys. Rev. B* **2007**, *75*, 205418.

(27) Eberlein, T.; Bangert, U.; Nair, R. R.; Jones, R.; Gass, M.; Bleloch, A. L.; Novoselov, K. S.; Geim, A.; Briddon, P. R. Plasmon Spectroscopy of Free-Standing Graphene Films. *Phys. Rev. B* **2008**, *77*, 233406.

(28) Kramberger, C.; Hambach, R.; Giorgetti, C.; Rümmeli, M. H.; Knupfer, M.; Fink, J.; Büchner, B.; Reining, L.; Einarsson, E.; Maruyama, S.; et al. Linear Plasmon Dispersion in Single-Wall Carbon Nanotubes and the Collective Excitation Spectrum of Graphene. *Phys. Rev. Lett.* **2008**, *100*, 196803.

(29) Gass, M.; Bangert, U.; Bleloch, A.; Wang, P.; Nair, R.; Geim, A. Free-Standing Graphene at Atomic Resolution. *Nat. Nanotechnol.* **2008**, *3*, 676−681.

(30) Jablan, M.; Buljan, H.; Soljačić, M. Plasmonics in Graphene at Infrared Frequencies. *Phys. Rev. B* **2009**, *80*, 245435.

(31) Mishchenko, E. G.; Shytov, A. V.; Silvestrov, P. G. Guided Plasmons in Graphene *p−n* Junctions. *Phys. Rev. Lett.* **2010**, *104*, 156806.

(32) Koppens, F. H. L.; Chang, D. E.; García de Abajo, F. J. Graphene Plasmonics: A Platform for Strong Light−Matter Interactions. *Nano Lett.* **2011**, *11*, 3370−3377.

(33) Thongrattanasiri, S.; Manjavacas, A.; García de Abajo, F. J. Quantum Finite-Size Effects in Graphene Plasmons. *ACS Nano* **2012**, *6*, 1766−1775.

(34) Nikitin, A. Y.; Guinea, F.; García-Vidal, F. J.; Martín-Moreno, L. Edge and Waveguide Terahertz Surface Plasmon Modes in Graphene Microribbons. *Phys. Rev. B* **2011**, *84*, 161407.

(35) Vakil, A.; Engheta, N. Transformation Optics Using Graphene. *Science* **2011**, *332*, 1291−1294.

(36) Wang, W.; Apell, P.; Kinaret, J. Edge Plasmons in Graphene Nanostructures. *Phys. Rev. B* **2011**, *84*, 085423.

(37) Ju, L.; Geng, B.; Horng, J.; Girit, C.; Martin, M.; Hao, Z.; Bechtel, H.; Liang, X.; Zettl, A.; Shen, Y.; et al. Graphene Plasmonics for Tunable Terahertz Metamaterials. *Nat. Nanotechnol.* **2011**, *6*, 630−634.

(38) Christensen, J.; Manjavacas, A.; Thongrattanasiri, S.; Koppens, F. H. L.; García de Abajo, F. J. Graphene Plasmon Waveguiding and Hybridization in Individual and Paired Nanoribbons. *ACS Nano* **2012**, *6*, 431−440.

(39) Wu, J.; Pisula, W.; Muellen, K. Graphenes as Potential Material for Electronics. *Chem. Rev.* **2007**, *107*, 718−747.

(40) Yang, X.; Dou, X.; Rouhanipour, A.; Zhi, L.; Rader, H. J.; Muellen, K. Two-Dimensional Graphene Nanoribbons. *J. Am. Chem. Soc.* **2008**, *130*, 4216.

(41) Cai, J.; Ruffieux, P.; Jaafar, R.; Bieri, M.; Braun, T.; Blankenburg, S.; Muoth, M.; Seitsonen, A. P.; Saleh, M.; Feng, X.; et al. Atomically Precise Bottom-Up Fabrication of Graphene Nanoribbons. *Nature* **2010**, *466*, 470−473.

(42) Palma, C.; Samorí, P. Blueprinting Macromolecular Electronics. *Nat. Chem.* **2011**, *3*, 431−436.

(43) Nakada, K.; Fujita, M.; Dresselhaus, G.; Dresselhaus, M. S. Edge State in Graphene Ribbons: Nanometer Size Effect and Edge Shape Dependence. *Phys. Rev. B* **1996**, *54*, 17954−17961.

(44) Ridley, J.; Zerner, M. An Intermediate Neglect of Differential Overlap Technique for Spectroscopy: Pyrrole and the Azines. *Theor. Chem. Acta* **1973**, *32*, 111−134.

(45) Caldas, M. J.; Pettenati, E.; Goldoni, G.; Molinari, E. Tailoring of Light Emission Properties of Functionalized Oligothiophenes. *Appl. Phys. Lett.* **2001**, *79*, 2505−2507.

(46) Wang, Z.; Tomović, Z.; Kastler, M.; Pretsch, R.; Negri, F.; Enkelmann, V.; Muellen, K. Graphitic Molecules with Partial "Zig/Zag" Periphery. *J. Am. Chem. Soc.* **2004**, *126*, 7794−7795.

(47) Cocchi, C.; Prezzi, D.; Ruini, A.; Caldas, M. J.; Molinari, E. Optical Properties and Charge-Transfer Excitations in Edge-Functionalized All-Graphene Nanojunctions. *J. Phys. Chem. Lett.* **2011**, *2*, 1315−1319.

(48) The reliability of the ZINDO model for the target systems was further demonstrated by computing time-dependent density functional theory (TDDFT-b3lyp) excitation energies and oscillator strengths for a selected flake of length ∼ 24 Å (GAMESS package with 3-21G basis set). For GAMESS package see: http://www.msg.ameslab.gov/gamess/ (accessed February 8, 2012).

(49) Dewar, M. J. S.; Zoebish, E. G.; Healy, E. F.; Stewart, J. J. P. A New General Purpose Quantum Mechanical Molecular Model. *J. Am. Chem. Soc.* **1985**, *107*, 3902−3909.

(50) Cocchi, C.; Ruini, A.; Prezzi, D.; Caldas, M. J.; Molinari, E. Designing All-Graphene Nanojunctions by Covalent Functionalization. *J. Phys. Chem. C* **2011**, *115*, 2969−2973.

(51) Shemella, P.; Zhang, Y.; Mailman, M.; Ajayan, P.; Nayak, S. Energy Gaps in Zero-Dimensional Graphene Nanoribbons. *Appl. Phys. Lett.* **2007**, *91*, 042101.

(52) Hod, O.; Barone, V.; Scuseria, G. E. Half-Metallic Graphene Nanodots: A Comprehensive First-Principles Theoretical Study. *Phys. Rev. B* **2008**, *77*, 035411.

(53) Prezzi, D.; Varsano, D.; Ruini, A.; Marini, A.; Molinari, E. Optical Properties of Graphene Nanoribbons: The Role of Many-Body Effects. *Phys. Rev. B* **2008**, *77*, 041404(R).

(54) The approximations included within the adopted ZINDO/S approach, specifically in the neglect of two center integrals, have to be taken into account in the calculation of $\rho^{0p}(\mathbf{r})$.

(55) Yan, J.; Yuan, Z.; Gao, S. End and Central Plasmon Resonances in Linear Atomic Chains. *Phys. Rev. Lett.* **2007**, *98*, 216602.

(56) Yan, J.; Gao, S. Plasmon Resonances in Linear Atomic Chains: Free-Electron Behavior and Anisotropic Screening of *d* Electrons. *Phys. Rev. B* **2008**, *78*, 235413.

(57) Lian, K.; Saɫek, P.; Jin, M.; Ding, D. Density-Functional Studies of Plasmons in Small Metal Clusters. *J. Chem. Phys.* **2009**, *130*, 174701.

(58) Yasuike, T.; Nobusada, K.; Hayashi, M. Collectivity of Plasmonic Excitations in Small Sodium Clusters with Ring and Linear Structures. *Phys. Rev. A* **2011**, *83*, 013201.

(59) Scholes, G.; Rumbles, G. Excitons in Nanoscale Systems. *Nat. Mater.* **2006**, *5*, 683−696.

(60) Matsuda, K.; Inoue, T.; Murakami, Y.; Maruyama, S.; Kanemitsu, Y. Exciton Dephasing and Multiexciton Recombinations in a Single Carbon Nanotube. *Phys. Rev. B* **2008**, *77*, 033406.

(61) Son, Y.-W.; Cohen, M. L.; Louie, S. G. Energy Gaps in Graphene Nanoribbons. *Phys. Rev. Lett.* **2006**, *97*, 216803.

(62) Barone, V.; Hod, O.; Scuseria, G. E. Electronic Structure and Stability of Semiconducting Graphene Nanoribbons. *Nano Lett.* **2006**, *6*, 2748−2754.

(63) Yang, L.; Cohen, M.; Louie, S. Excitonic Effects in the Optical Spectra of Graphene Nanoribbons. *Nano Lett.* **2007**, *7*, 3112−3115.

(64) Prezzi, D.; Varsano, D.; Ruini, A.; Molinari, E. Quantum Dot States and Optical Excitations of Edge-Modulated Graphene Nanoribbons. *Phys. Rev. B* **2011**, *84*, 041401.

929

dx.doi.org/10.1021/jz300164p | *J. Phys. Chem. Lett.* 2012, 3, 924−929